



# Self-noise prediction of a sharp-edged strut using a quasi-periodic CFD-BEM technique

Mahmoud Karimi<sup>1</sup>; Paul Croaker<sup>1</sup>; Nicole Kessissoglou<sup>1</sup>; Con Doolan<sup>2</sup>; Steffen Marburg<sup>3</sup>

<sup>1</sup> School of Mechanical and Manufacturing Engineering, UNSW Australia, Sydney, NSW 2052, Australia

<sup>2</sup> School of Mechanical Engineering, The University of Adelaide, Adelaide, SA 5005, Australia

<sup>3</sup> LRT4-Institute of Mechanics, Universität der Bundeswehr München, D-85579 Neubiberg, Germany

## ABSTRACT

The self-noise generated by a sharp-edged strut immersed in low Mach number flow is predicted using a hybrid computational fluid dynamics (CFD) - boundary element method (BEM) technique. The fluctuating flow field is obtained using an incompressible CFD solver. A high-order reconstruction scheme is used to extract acoustic sources based on Lighthill's analogy from the flow field data. Acoustic waves generated by these flow noise sources propagate to and are scattered by the trailing edge of the strut. A BEM model of the sharp-edged strut, based on the Burton-Miller formulation, is used to predict the scattered sound pressure. A quasi-periodic technique is implemented in the BEM model so that the sound generated by the entire span of the strut can be predicted by modelling only a small spanwise segment. The results from the hybrid CFD-BEM technique are presented for turbulent flow past a sharp-edged strut, with Reynolds number based on chord  $Re_c=2.0 \times 10^5$  and Mach number  $M=0.044$ . The computed aerodynamic and acoustic results are compared with experimental data obtained using the anechoic wind tunnel at the University of Adelaide.

Keywords: Trailing edge noise, computational fluid dynamics, boundary element method  
I-INCE Classification of Subjects Number(s): 21.6.4

## 1. INTRODUCTION

Airfoil trailing edge noise is one of the most significant current challenges in aeroacoustic research; this phenomenon occurs in many practical applications such as aircraft wings, gas-turbine blades, wind turbines, helicopter rotors, cooling fans, propellers and submarine control surfaces. Scattering of the acoustic pressure fluctuations induced by boundary layer turbulent structures over the trailing edge geometry produces trailing edge noise. One of the first systematic studies of trailing edge noise was reported by Ffowcs Williams and Hall (1) based on the classical Lighthill analogy (2). They analyzed the turbulent eddies past a sharp edge, such as encountered at the trailing edge of an airfoil. A theoretical model based on a vanishingly thin half plane of infinite extent was developed. It was identified that the far-field sound intensity for trailing edge noise had a scaling of  $M^5$ . It was also realized that the mechanism responsible for this trailing edge noise is the scattering and diffraction of the flow induced acoustic waves by the thin trailing edge. Amiet (3) proposed a trailing edge noise model using the convecting surface pressure spectrum upstream of the trailing edge as the input and a rigid semi-infinite plate as the scattering body. Howe (4) demonstrated that Amiet's trailing edge noise model leads to the same  $M^5$  scaling that was reported by Ffowcs Williams and Hall (1).

Howe (5) and Roger and Moreau (6, 7) developed advanced analytical models of trailing edge noise which account for the finite chord length and finite thickness of the airfoil. To better understand the mechanisms of generating trailing edge noise, Moreau and Roger (8) experimentally measured the static surface pressure at the mid span of an airfoil and applied these pressure spectra to their trailing edge noise model. They demonstrated that their model produces very similar results to the model proposed by Howe (5). Furthermore, comparison of the measured far-field spectra with numerical results of Oberai et al. (9) revealed similar directivity, but with an overprediction of the sound pressure amplitude (8). Moreau et al. (10, 11, 12, 13) conducted a number of aeroacoustic experiments on sharp-edged flat plates in an anechoic wind tunnel at low-to-moderate Reynolds number. They examined a variety of semi-empirical methods for predicting trailing edge noise which were shown to underestimate noise at lower frequencies (10).

<sup>1</sup> m.karimi@student.unsw.edu.au

Wang and Moin (14) performed an incompressible large eddy simulation of turbulent flow over a flat strut, with the predicted hydrodynamics comparing well with the experiments conducted by Blake (15). They then predicted the far-field sound pressure using the method of Ffowcs Williams and Hall (1), which requires as an input the Lighthill tensor distribution well within one acoustic wavelength of the trailing edge. No acoustic measurements were conducted during the original experiments and hence no validation of the far-field sound pressures obtained from the simulations was possible. Wang et al. (16) conducted a similar hybrid LES - acoustic analogy simulation on the cambered airfoil of an industrial fan blade. They applied a finite chord correction to the trailing edge noise model of Ffowcs Williams and Hall (1), following the multiple scattering analysis of Howe (5). Manoha et al. (17) performed LES of trailing edge flow and computed the radiated noise using Lighthill's acoustic analogy. The aerodynamic results clearly demonstrated the strongly three-dimensional character of the flow, with the onset of a vortex-shedding mechanism occurring at a frequency in agreement with theoretical and experimental data. Moon et al. (18) adopted a hybrid large eddy simulation (LES) / linearized perturbed compressible equations (LPCE) technique to predict low-subsonic, turbulent flow noise of a flat plate at zero angle of attack. The noise sources in the near wall turbulence or in the wake were computed by the incompressible LES, while the generation and propagation of the acoustic waves were solved by the LPCE.

Khalighi et al. (19) developed a boundary integral equation from Lighthill's wave equation which was solved using the boundary element method (BEM). The method was applied to predict the sound pressure field radiated by turbulent flow past a cylinder and an automotive side mirror, as well as the trailing edge noise from an airfoil (20). For all cases, the predicted radiated sound field matched well with experimental measurements. The approach by Khalighi et al. (19) is an accurate method to predict low Mach number flow induced noise in the presence of both acoustically compact or non-compact bodies. However, the propagation of the acoustic waves produced by the hydrodynamic noise sources to the body were incorporated directly in the authors' own BEM solver, which relied on the combined Helmholtz integral equation formulation known as the CHIEF method (21) to deal with the irregular frequencies that are encountered in exterior BEM problems. Marburg and Amini (22) showed that the Burton and Miller method (23) is a more reliable and robust method to remove the irregular frequencies compared to the CHIEF method. Recently, Croaker et al. (24) used a hybrid CFD-BEM technique to identify the scattering of sound waves produced by laminar vortex shedding from a two-dimensional cylinder. The total far-field sound pressure level included both the scattered field and the radiation due to the viscous shear stress dipoles.

In this work, the self-noise generated by a sharp-edged plate immersed in low Mach number flow is predicted using a hybrid CFD-BEM technique. The procedure is divided into three steps as follows. First, the unsteady incompressible flow field past a flat plate with a sharp trailing edge is simulated using an LES method. Second, the acoustic field is computed using Lighthill's analogy by extracting sources from the unsteady flow data. The incident acoustic field is then applied to a BEM method based on the Burton-Miller formulation to predict the scattered sound pressure. A quasi-periodic technique is implemented in the BEM model so that the sound generated by the entire span of the strut can be predicted by modelling only a small spanwise segment. The results from the hybrid CFD-BEM technique are presented for turbulent flow past a sharp-edged strut, with Reynolds number based on chord  $Re_c=2.0 \times 10^5$  and Mach number  $M=0.044$ . The computed aerodynamic and acoustic results are compared with experimental data obtained using the anechoic wind tunnel at the University of Adelaide.

## 2. NUMERICAL MODEL

### 2.1 Boundary Element Formulation

The non-homogeneous Helmholtz equation is given by

$$\Delta p(\mathbf{x}) + k^2 p(\mathbf{x}) = -F \quad (1)$$

where  $p(\mathbf{x})$  is the acoustic pressure at field point  $\mathbf{x}$ ,  $F$  is the source,  $\Delta$  is the Laplacian operator,  $k = \omega/c$  is the acoustic wave number,  $\omega$  is the angular frequency and  $c$  is the speed of sound. The non-homogenous Helmholtz equation can be written in a weak formulation after integrating by parts twice as follows (25)

$$c(\mathbf{x})p(\mathbf{x}) + \int_{\Gamma} \frac{\partial G(\mathbf{x}, \mathbf{y})}{\partial n(\mathbf{y})} p(\mathbf{y}) d\Gamma(\mathbf{y}) = \tilde{i}\omega\rho_0 \int_{\Gamma} G(\mathbf{x}, \mathbf{y}) v_f(\mathbf{y}) d\Gamma(\mathbf{y}) + p_{\text{inc}}(\mathbf{x}) \quad (2)$$

where  $\rho_0$  is fluid density and  $\tilde{i} = \sqrt{-1}$  is the imaginary unit. The vector  $\mathbf{n}(\mathbf{y})$  represents the outward normal vector at the point  $\mathbf{y}$ ,  $\partial/\partial n(\mathbf{y})$  is the normal derivative and  $\mathbf{y}$  is a source point position on the boundary  $\Gamma$ . Solution of the non-homogenous Helmholtz equation can be obtained by calculating the incident acoustic

pressure radiated by the source and applying it as a load to the boundary integral equation (2).  $p_{\text{inc}}(\mathbf{x})$  is the acoustic pressure incident as a result of the acoustic source.  $c(\mathbf{x})$  is a free-term coefficient and equals 1 in the domain interior and 0.5 on a smooth boundary.  $G(\mathbf{x}, \mathbf{y})$  is the free-space Green's function for the Helmholtz equation given by

$$G(\mathbf{x}, \mathbf{y}) = \frac{e^{i\tilde{k}r}}{4\pi r} \quad \text{where} \quad r = |\mathbf{x} - \mathbf{y}| \quad (3)$$

The fluid particle velocity  $v_f(\mathbf{x})$  is related to the normal derivative of the acoustic pressure as follows

$$v_f(\mathbf{x}) = \frac{1}{i\omega\rho_0} \frac{\partial p(\mathbf{x})}{\partial n(\mathbf{x})} \quad (4)$$

It has been demonstrated that equation (2) has a major flaw for exterior acoustic applications; that is, it fails to have a unique solution at certain so-called irregular frequencies (22). Burton and Miller (23) showed that a remedy to this problem is to use the linear combination of equation (2) in conjunction with its differentiated form. This will lead to a unique solution for exterior acoustic problems at all frequencies. Taking the derivative of the integral equation (2) with respect to the normal at point  $\mathbf{x}$ , the following hyper-singular boundary integral equation produces

$$i\omega\rho_0 c(\mathbf{x})v_f(\mathbf{x}) + \int_{\Gamma} \frac{\partial^2 G(\mathbf{x}, \mathbf{y})}{\partial n(\mathbf{x})\partial n(\mathbf{y})} p(\mathbf{y}) d\Gamma(\mathbf{y}) = i\omega\rho_0 \int_{\Gamma} \frac{\partial G(\mathbf{x}, \mathbf{y})}{\partial n(\mathbf{x})} v_f(\mathbf{y}) d\Gamma(\mathbf{y}) + \frac{\partial p_{\text{inc}}(\mathbf{x})}{\partial n(\mathbf{x})} \quad (5)$$

The Burton and Miller formulation can then be expressed by

$$c(\mathbf{x})p(\mathbf{x}) + \int_{\Gamma} \frac{\partial G(\mathbf{x}, \mathbf{y})}{\partial n(\mathbf{y})} p(\mathbf{y}) d\Gamma(\mathbf{y}) + \beta \int_{\Gamma} \frac{\partial^2 G(\mathbf{x}, \mathbf{y})}{\partial n(\mathbf{x})\partial n(\mathbf{y})} p(\mathbf{y}) d\Gamma(\mathbf{y}) = i\omega\rho_0 \left\{ \int_{\Gamma} G(\mathbf{x}, \mathbf{y})v_f(\mathbf{y}) d\Gamma(\mathbf{y}) - \beta \left[ c(\mathbf{x})v_f(\mathbf{x}) - \int_{\Gamma} \frac{\partial G(\mathbf{x}, \mathbf{y})}{\partial n(\mathbf{x})} v_f(\mathbf{y}) d\Gamma(\mathbf{y}) \right] \right\} + p_{\text{inc}}(\mathbf{x}) + \beta \frac{\partial p_{\text{inc}}(\mathbf{x})}{\partial n(\mathbf{x})} \quad (6)$$

where  $\beta$  is the coupling parameter that determines the relative weights of equations (2) and (5). A unique solution to equation (6) exists for all non-zero complex values of  $\beta$ . Rigorous mathematical analysis by Amini (26) revealed that a good choice for the coupling parameter was  $\beta = \tilde{i}/k$ .

## 2.2 Incident Field from Lighthill's Analogy

For flow-induced noise problems (2), the source  $F$  in equation (1) can be replaced with

$$F = \frac{\partial^2 T_{ij}}{\partial y_i \partial y_j} \quad (7)$$

where  $T_{ij} = \rho_0 u_i u_j$  is approximate Lighthill's tensor (at low Mach number), and  $u_i, u_j$  are the  $i^{\text{th}}$  and  $j^{\text{th}}$  components of the velocity vector, respectively. The particular solution of non-homogenous Helmholtz equation due to this source can be expressed by

$$p_{\text{inc}}(\mathbf{x}) = \int_{\Omega} \frac{\partial^2 T_{ij}(\mathbf{y})}{\partial y_i \partial y_j} G(\mathbf{x}, \mathbf{y}) d\mathbf{y} \quad (8)$$

where  $\Omega$  is the acoustic domain. As can be seen from equation (5), using the Burton and Miller method requires that the incident pressure gradient to be determined on the surface of the body, which can be derived from equation (8) as follows

$$\frac{\partial p_{\text{inc}}(\mathbf{x})}{\partial n(\mathbf{x})} = \int_{\Omega} \frac{\partial^2 T_{ij}(\mathbf{y})}{\partial y_i \partial y_j} \frac{\partial G(\mathbf{x}, \mathbf{y})}{\partial n(\mathbf{x})} d\mathbf{y} \quad (9)$$

Equations (8) and (9) are solved using the formulations for near-field pressure and pressure gradient derived by Croaker et al. (?). In this study, the sound pressure must satisfy the Sommerfeld radiation condition in the far field as well as the Neumann boundary condition on the surface of the plate. The latter condition implies that the plate is considered rigid with zero admittance. Therefore, the boundary condition can be expressed as follows

$$v_f(\mathbf{y}) = 0, \quad \mathbf{y} \in \Gamma \quad (10)$$

### 2.3 Quasi-Periodic Boundary Element Method

A quasi-periodic technique is implemented in the BEM model so that the sound generated by the entire surface of a body can be predicted by modelling only a small segment of body. To do this, the surface of the body is divided into  $(2N + 1)$  sections. Hence, the total length of the body is given by

$$L = (2N + 1)x_p \quad (11)$$

where  $x_p$  is the length of each section.  $N$  is the number of sections on each side of the middle section  $\Gamma_0$ .

Assuming a periodic solution for the acoustic pressure such as  $p(\mathbf{y}) = p(\mathbf{y} + n\mathbf{d})$ , the boundary  $\Gamma$  is divided as follows

$$\Gamma = \Gamma_{-N} \cup \Gamma_{-N+1} \cup \dots \cup \Gamma_{-1} \cup \Gamma_0 \cup \Gamma_1 \cup \dots \cup \Gamma_n \cup \dots \cup \Gamma_{N-1} \cup \Gamma_N \quad (12)$$

where  $\mathbf{d}$  is a vector from a collocation point of one boundary section to its adjacent boundary section. The length of  $\mathbf{d}$  is equal to  $x_p$ .

With the assumption of a periodic solution as well as considering the Neumann boundary condition, equations (2) and (5) can be respectively rewritten as follows

$$c(\mathbf{x})p(\mathbf{x}) + \sum_{n=-N}^N \left[ \int_{\Gamma_n} \frac{\partial G(\mathbf{x}, \mathbf{y}_n)}{\partial n(\mathbf{y}_n)} p(\mathbf{y}) d\Gamma_n(\mathbf{y}_n) \right] = p_{\text{inc}}(\mathbf{x}), \quad \mathbf{y} \in \Gamma_0 \quad (13)$$

$$\sum_{n=-N}^N \left[ \int_{\Gamma_n} \frac{\partial^2 G(\mathbf{x}, \mathbf{y}_n)}{\partial n(\mathbf{x}) \partial n(\mathbf{y}_n)} p(\mathbf{y}) d\Gamma_n(\mathbf{y}_n) \right] = \frac{\partial p_{\text{inc}}(\mathbf{x})}{\partial n(\mathbf{x})} = q_{\text{inc}}(\mathbf{x}), \quad \mathbf{y} \in \Gamma_0 \quad (14)$$

where  $q_{\text{inc}}$  represents the incident pressure gradient, the acoustic pressure on each element can be discretised as follows

$$p(\mathbf{y}) = \sum_{i=1}^M \Phi_i(\mathbf{y}) p_i \quad (15)$$

where  $\Phi_i(\mathbf{y})$  are interpolation functions and  $p_i$  represents the sound pressure at nodal points. In the case of a quasi-periodic assumption, only collocation points of the elements located on  $\Gamma_0$  need to be included in the computation. This is sufficient since the quasi-periodic assumption leads to a situation where collocation points of other sections only provide redundant information. Assembling nodal values of  $p$ ,  $p_{\text{inc}}$  and  $q_{\text{inc}}$  in vectors  $\mathbf{p}$ ,  $\mathbf{p}_{\text{inc}}$  and  $\mathbf{q}_{\text{inc}}$ , respectively, then substituting equation (15) into equations (13) and (14), the quasi-periodic BEM formulation based on Burton and Miller method is obtained as the following linear system of equations:

$$(\mathbf{H} + \beta \mathbf{D})\mathbf{p} = \mathbf{p}_{\text{inc}} + \beta \mathbf{q}_{\text{inc}} \quad (16)$$

Using this quasi-periodic BEM model, the acoustic pressure  $p$  radiated from flow sources and scattered by the body is predicted.

### 2.4 Large Eddy Simulation

To accurately predict the trailing edge noise, the fluid dynamics has to be adequately resolved for noise-generating eddies over a wide range of length scales. This aim cannot be fulfilled by employing traditional CFD methods based on Reynolds-averaged Navier-Stokes (RANS) equations. Large eddy simulation (LES) is a well-established method to determine the acoustic sources, since it resolves only large-scale eddies from fluctuating flow field, which are known to have significant contributions to noise generation. The effect of small (subgrid) scale eddies on the large-scale eddies is modelled. Hence, LES decreases the computational cost in comparison to direct numerical simulation (DNS).

To demonstrate the effectiveness of the approach adopted in this work, a flat plate model was used which corresponds to the experiment conducted by Moreau et al. (10) in an anechoic wind tunnel. The flat plate used in both the experiment and simulation has a chord of 200 mm, a span of 450 mm, and a thickness of 5 mm. The leading edge is circular with a diameter of 5 mm while the trailing edge is a symmetric wedge shape with an apex angle of  $12^\circ$ , as shown in Figure 1. In the experimental test, the flat plate was tested with zero angle of attack and the radiated sound pressure was measured at three positions, one above the trailing edge, one below the trailing edge and one above the leading edge.

Incompressible flow field past the flat plate is simulated at a Reynolds number based on chord  $Re_c = 2.0 \times 10^5$  and Mach number  $M = 0.044$ . At this Reynolds number the flow is in the turbulent unsteady regime and is three

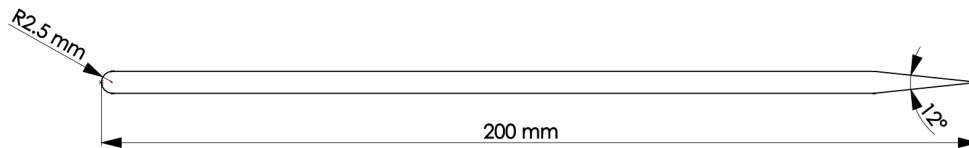


Figure 1 – Flat plate dimensions

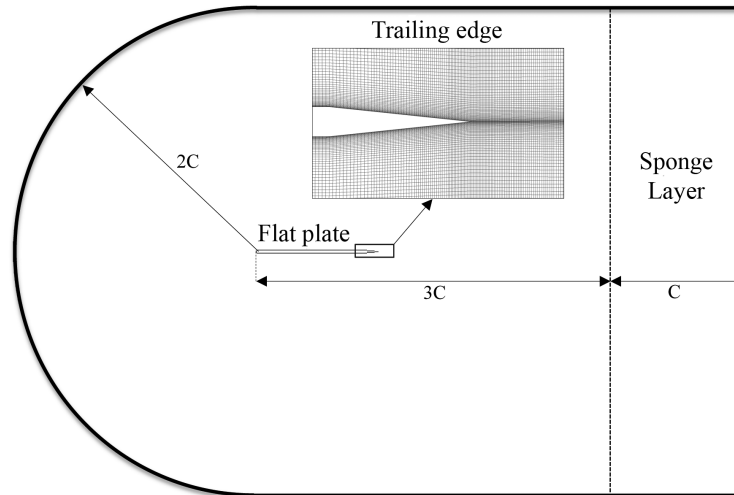


Figure 2 – Schematic diagram of shape and size of CFD domain

dimensional. The LES simulation is performed in Fluent on a C-grid domain with nearly 3 million hexahedral cells. A relatively large computational domain is used to minimize the boundary condition influence, which is extended two chords above and below the plate as well as upstream and downstream. A sponge layer extends the computational domain in the downstream direction for an additional chord as shown in Figure 2. The mesh distribution is biased so that the region near the plate and also the wake region contains a high cell density to resolve eddies and fluctuations. Apart from vicinity of leading edge, the resolution of the near-wall grid on the plate is  $\Delta x^+ \leq 29$ ,  $\Delta y^+ \leq 1$  and  $\Delta z^+ \leq 4.7$ . The cell size in the sponge layer grows rapidly in the  $x$ -direction. The sponge layer is implemented to allow the vortical disturbances in the wake to leave the computational domain smoothly. This has been done by defining a cosine function of  $x$  which increases the viscosity through the layer.

The inlet velocity is set to 15 m/s on the semi-circular boundary, while a zero average pressure is imposed at the outlet. A no-slip condition is applied on the surface of the plate, and the top and bottom boundaries are considered as free-slip walls. It should be noted that a spanwise extension is selected as 3% of the plate chord with flow periodicity assumed at the side boundaries. The calculation procedure is described as follows. First, a transient simulation based on Menter's shear-stress transport (SST)  $k - \omega$  model was done as an initial condition for the LES. The LES simulation was allowed to progress until the flow field had become quasi-periodic in time. Velocity components from the LES are then extracted to calculate the sound sources. Since these sources are in the time domain, a discrete Fourier transform (DFT) is performed to transfer the data into the frequency domain. Equations (8) and (9) are then solved to predict the incident pressure and pressure gradient on the surface of the plate. Once the incident pressure and its gradient are obtained, the total sound pressure can be computed from the BEM formulation given by equation (16).

### 3. RESULTS AND DISCUSSION

#### 3.1 Vorticities at the Trailing Edge

To visualize the vortex regions within the boundary layer and at the trailing-edge, the  $Q$ -criterion is employed as an indication of balance between strain rate and vorticity magnitude (27). For incompressible flow the  $Q$ -criterion can be written as  $Q = (\|\Lambda\|^2 - \|\mathbf{S}\|^2)/2$ , where  $\|\Lambda\| = \sqrt{\text{tr}(\Lambda\Lambda^T)}$  and  $\|\mathbf{S}\| = \sqrt{\text{tr}(\mathbf{S}\mathbf{S}^T)}$ .  $\mathbf{S}$  and  $\Lambda$  are symmetric and skew-symmetric components of the velocity gradient tensor  $\nabla\mathbf{u}$ , respectively. The  $Q$ -criterion identifies vortices as regions where the vorticity magnitude is larger than the magnitude of strain rate. Figure 3 shows the iso-surfaces of the second invariant of the velocity gradient tensor; where  $h$  is the plate thickness and  $U_\infty$  is the free-stream velocity. It can be observed that sound sources are located at the vicinity of trailing edge and in the wake where the flow structures are aggregated.

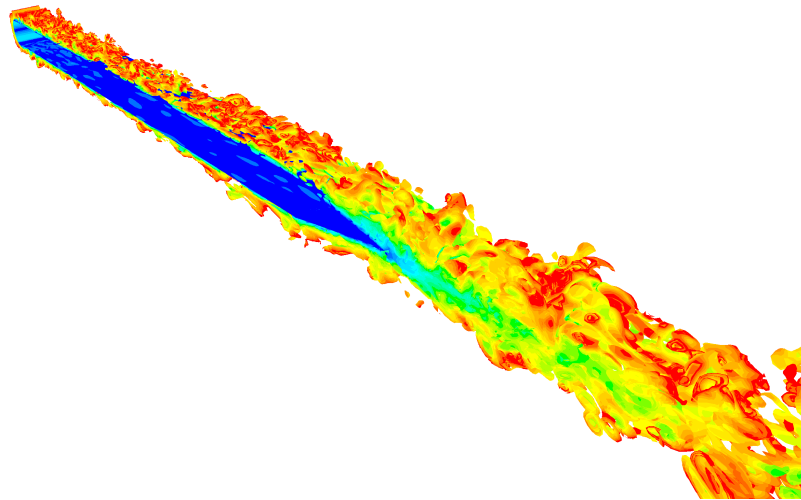


Figure 3 – Flow structures over the flat plate at  $Re_c=2.0 \times 10^5$  and Mach number  $M=0.044$ ; Iso-surface of  $Q = 0.2$ , non-dimensionalised by  $(U_\infty/h)^2$

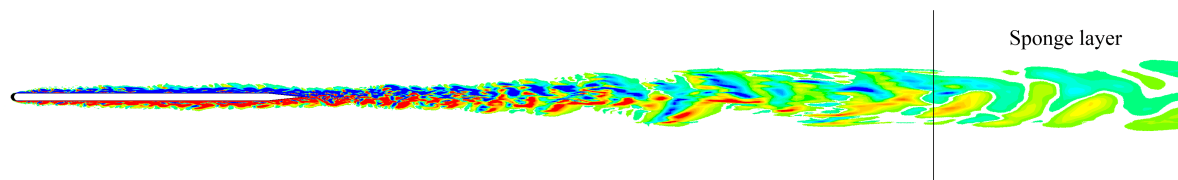


Figure 4 – Instantaneous spanwise vorticity contours at the mid-span

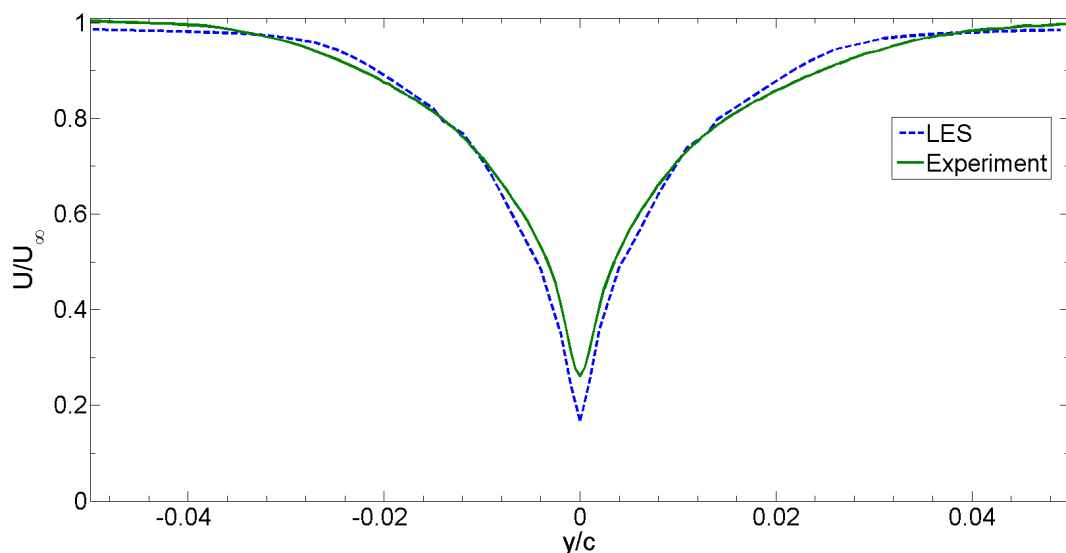


Figure 5 – Normalized mean velocity profile ( $U/U_\infty$ ) measured in the near wake of the flat plate

The instantaneous spanwise vorticity over the flat plate is shown in Figure 4. To illustrate the effectiveness of the sponge layer on damping out the vorticity, a vertical line has been drawn which denotes where the sponge layer begins. It can be seen that the vorticity contours are smooth, which demonstrates that the implementation of the sponge layer was successful at preventing reflection of vorticity from the downstream boundary.

### 3.2 Velocity Profile and Spectra at the Trailing Edge

A comparison between the mean velocity profile extracted from LES and the mean velocity profile obtained experimentally from wind tunnel measurements at the University of Adelaide is depicted in Figure 5, where  $U$  is the mean velocity. Good agreement between numerical results obtained in this work and experimental results by Moreau et al. (10) can be observed. The velocity was measured in the vertical direction  $y$  at a constant  $x$  position of 0.7 mm from the trailing edge. Figure 5 shows that the velocity profile is mostly symmetric about the trailing edge. The LES results reveal that the circular leading edge produces a laminar separation bubble. The reattachment of the flow after this separation bubble is highly unstable and generates significant turbulent fluctuations in the flow. Downstream of the reattachment the turbulent boundary layer continues to develop.

The spectra of fluctuating velocity are presented in Figure 6 at two different positions in the wake of the flat plate. Figure 6(a) shows the velocity spectra adjacent to the trailing edge. For this case the CFD results are in very good agreement with experimental data. At a position further from the trailing edge as shown in Figure 6(b) the CFD results diverge from experimental data at frequencies above around 2 kHz. This discrepancy can be attributed to the mesh distribution in the downstream region. The cell size in the wake increases in the  $x$ -direction. Hence, at a position further from the trailing edge, the grid resolution was not sufficient to appropriately predict the velocity fluctuation at high frequencies.

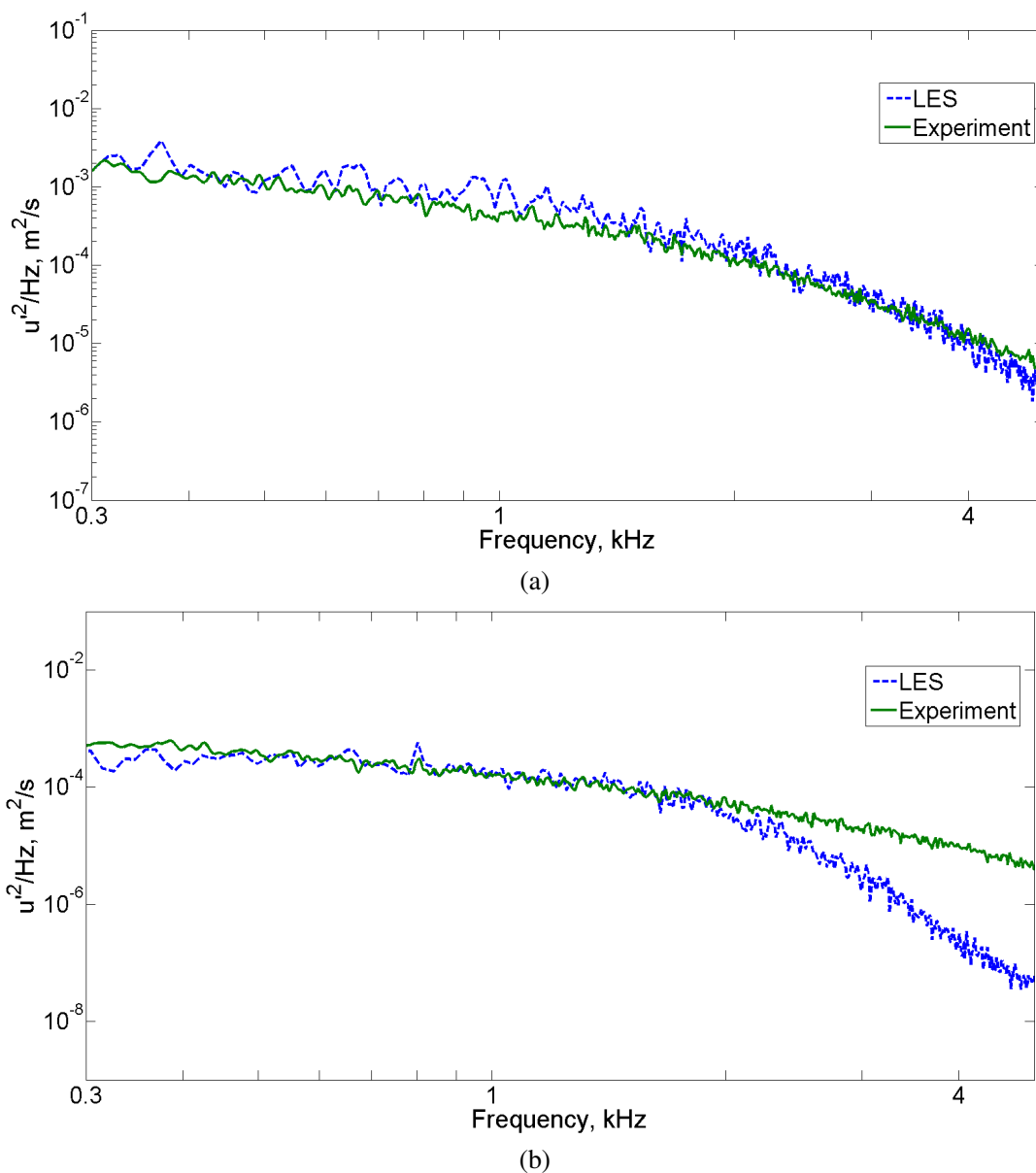


Figure 6 – The velocity spectra for the flat plate near the trailing edge at  $y/c=-0.0035$ ; (a)  $x/c=0.01$  and (b)  $x/c=0.2$

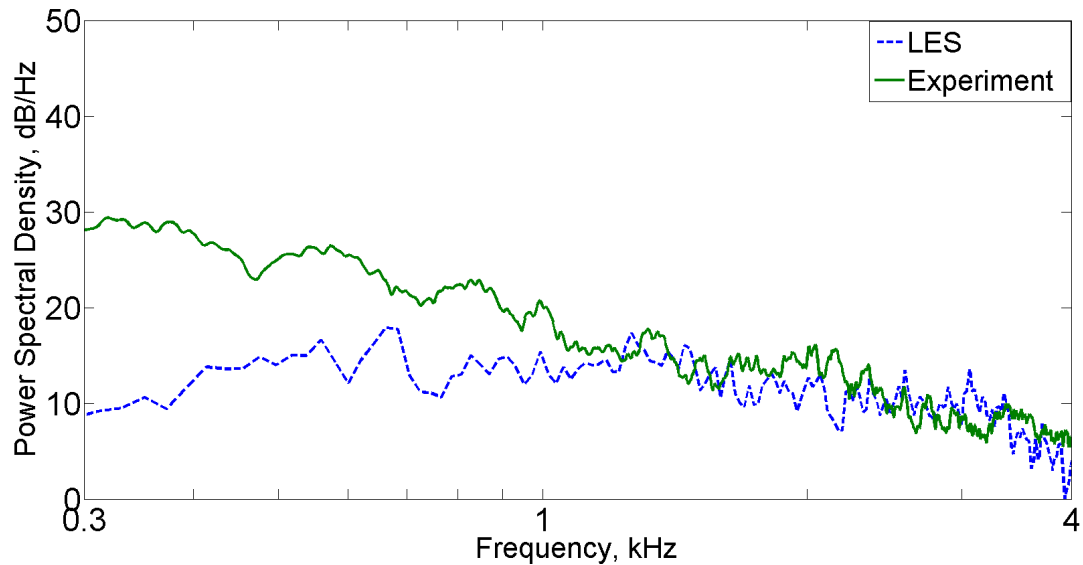


Figure 7 – Comparison of experimental and numerical far-field acoustic spectra

### 3.3 Far-Field Acoustic Pressure

In Figure 7, the broadband noise radiated by the flat plate predicted using the quasi-periodic boundary element method is compared with experimental results. The sound pressure is computed at two positions corresponding to above and below the trailing edge, which are the locations of microphones in the experiment (13). The sound pressure measured by the two microphones are equal in magnitude, highly correlated and  $180^\circ$  out of phase. To isolate the trailing edge noise in the measurements, the out-of-phase signals should be subtracted. An offset value of 6 dB also needs to be removed from the corrected trailing edge noise spectra when using this method (13). The power spectral density of the calculated pressure is shown in Figure 7. It should be noted that the lower and the upper limit of confidence interval in the measured spectrum are  $-1.14$  and  $+1.01$  dB/Hz, respectively. Figure 7 shows that the numerical results are in good agreement with experimental data at high frequencies. Nonetheless, there is a considerable difference between the numerical and experimental results at low frequencies. According to the Corcos model (6), the spanwise coherence length can be estimated by  $L_c(\omega) \approx 2.1U_c/\omega$ , where  $U_c$  is the convection speed. According to this model and considering the fact that the segment length used in the CFD simulation was only 3% of the plate chord (6 mm), the current simulated segment length cannot resolve the correct behaviour of the flow structures with frequencies less than 670 Hz. To obtain reasonable results at all frequencies between 300 Hz and 4 kHz, the minimum span of 14 mm should be implemented in the simulation. However, using the current span it is possible to reasonably predict the sound pressure at high frequencies.

## 4. CONCLUSIONS

A hybrid computational fluid dynamics (CFD) - boundary element method (BEM) technique was used to predict the self-noise generated by a sharp-edged strut immersed in low Mach number flow. In this work, the propagated acoustic waves generated by the flow noise sources as well as the scattering and diffraction waves from the entire strut were taken into account. A BEM model of the sharp-edged strut, based on the Burton-Miller formulation, was used to predict the scattered sound pressure. A quasi-periodic technique was implemented in the BEM model to significantly reduce the computational cost of the boundary element method. Using this approach, the sound generated by the entire span of the strut can be predicted by modelling only a small spanwise segment. The results from the hybrid CFD-BEM technique were presented for turbulent flow past a sharp-edged strut and the computed aerodynamic and acoustic results were compared with experimental data obtained using the anechoic wind tunnel at the University of Adelaide. A comparison of the numerical results obtained in this work and the experimental results obtained previously suggests that to accurately predict the sound pressure, a finer mesh is required in the wake of the strut and a longer span should be implemented in the CFD simulation.

## REFERENCES

1. Ffowcs Williams JE, Hall LH. Aerodynamic sound generation by turbulent flow in the vicinity of a scattering half plane. *J Fluid Mech.* 1970;40(4):657–670.
2. Lighthill MJ. On sound generated aerodynamically. *Proc Soc Roy Soc A.* 1952;211:564–587.
3. Amiet R. Noise due to turbulent flow past a trailing edge. *J Sound Vib.* 1976;47(3):387–393.
4. Howe M. A review of the theory of trailing edge noise. *J Sound Vib.* 1978;61(3):437–465.
5. Howe M. Edge-source acoustic Green's function for an airfoil of arbitrary chord with application to trailing-edge noise. *Q J Mech Appl Math.* 2001;54:139–155.
6. Roger M, Moreau S. Broadband self-noise from loaded fan blades. *AIAA J.* 2004;42:536–544.
7. Roger M, Moreau S. Back-scattering correction and further extension of Amiet's trailing-edge noise model. Part I: Theory. *J Sound Vib.* 2005;286:477–506.
8. Moreau S, Roger M. Back-scattering correction and further extensions of Amiet's trailing-edge noise model. Part II: Application. *J Sound Vib.* 2009;323:397–425.
9. Oberai A, Roknaldin F, Hughes TJR. Computation of trailing edge noise due to turbulent flow over an airfoil. *AIAA J.* 2002;40:2206–2216.
10. Moreau DJ, Brooks L, Doolan CJ. Broadband trailing edge noise from a sharp-edged strut. *J Acoust Soc Am.* 2011;129(5):2820–9.
11. Moreau DJ, Brooks L, Doolan CJ. Experimental investigation of broadband trailing edge noise from sharp-edged struts. *Proc 17th AIAA/CEAS Aeroacoustics Conference (32nd AIAA Aeroacoustics Conference).* 2011;5-8 June, Portland, Oregon.
12. Moreau DJ, Doolan CJ. Noise-reduction mechanism of a flat-plate serrated trailing edge. *AIAA J.* 2013;51(10):2513–2522.
13. Moreau DJ, Brooks L, Doolan CJ. The effect of boundary layer type on trailing edge noise from sharp-edged flat plates at low-to-moderate Reynolds number. *J Sound Vib.* 2012;331(17):3976–3988.
14. Wang M, Moin P. Computation of trailing-edge flow and noise using large-eddy simulation. *AIAA J.* 2000;38:2201–2209.
15. Blake WK. A statistical description of pressure and velocity fields at the trailing edge of a flat strut. David Taylor Naval Ship R & D Center, Maryland; 1975. 4241.
16. Wang M, Moreau S, Iaccarino G, Roger M. LES prediction of wall-pressure fluctuations and noise of a low-speed airfoil. *Int J Aeroacoust.* 2009;8(3):177–198.
17. Manoha E, Troff B, Sagaut P. Trailing-edge noise prediction using large-eddy simulation and acoustic analogy. *AIAA J.* 2000;38(4):575–583.
18. Moon YJ, Seo JH, Bae YM, Roger M, Becker S. A hybrid prediction method for low-subsonic turbulent flow noise. *Comput Fluids.* 2010;39:1125–1135.
19. Khalighi Y, Mani A, Ham F, Moin P. Prediction of sound generated by complex flows at low Mach numbers. *AIAA J.* 2010;48(2):306–316.
20. Khalighi Y. *Computational Aeroacoustics of Complex Flows at Low Mach Number.* Stanford University; 2010.
21. Schenk HA. Improved integral formulation for acoustic radiation problems. *J Acoust Soc Am.* 1968;44:41–58.
22. Marburg S, Amini S. Cat's eye radiation with boundary elements: Comparative study on treatment. *J Comput Acoust.* 2005;13:21–45.
23. Burton AJ, Miller GF. The application of integral equation methods to the numerical solution of some exterior boundary-value problems. *Proc Roy Soc Lon Ser A.* 1971;323:201–210.

24. Croaker P, Kessissoglou N, Marburg S. A CFD-BEM coupling technique for low Mach number flow induced noise. Proc Acoustics 2013;17-20 November 2013, Victor Harbor, Australia, 2013.
25. Marburg S, Nolte B. Computational acoustics of noise propagation in fluids - Finite and boundary element methods. Springer; 2008.
26. Amini S. On the choice of the coupling parameter in boundary integral formulations of the exterior acoustics problem. Appl Anal. 1990;35:75–92.
27. Chakraborty P, Balachandar S, Ronald A. On the relationships between local vortex identification schemes. J Fluid Mech. 2005;535:189–214.